Electronic Supplementary information (ESI) *for*

Core-dependent Growth of Platinum Shell Nanocrystals and Their Electrochemical Characteristics for Fuel Cells

Tsan-Yao Chen[a,b*], *I-Li Chen*[c], *Yu-Ting Liu*[d], *Tsang-Lang Lin*[a], *Po-Wei Yang*[a], *Chiun-Yi Wu*[a], *Chi-Chang Hu*[b], *T.-J. Mark Luo*[b], *and Chih-Hao Lee*[a,e*]

Affiliation:

[a.] Department of Engineering and System Science, National Tsing Hua University, Hsinchu 30013, Taiwan

[b.] Department of Materials Science, North Carolina State University, Raleigh 27695, USA

[c.] Department of Civil and Environment Engineering, Duke University, Durham, NC, USA

[d.] Department of Chemical Engineering, National Tsing Hua University, Hsinchu 30013, Taiwan

[e.] National Synchrotron Radiation Research Center, Hsinchu 30076, Taiwan

[*]To whom correspondence should be addressed: Tsan-Yao Chen, email: chencaeser@gmail.com; Chi-Hao Lee, email: chlee@mx.nthu.edu.tw; Tel: +886-3-5742671 (O); +886-3-5728445 (Fax)

1. X-ray absorption spectroscopy data collection and analysis

XAS data collection. The Co *K*-edge (7709 eV) and Ru *K*-edge (22117 eV) X-ray absorption spectra of Pt_S/Co_C and Pt_S/Ru_C NPs were recorded using the wiggler beamline at BL-17C1 and the superconducting wavelength shifter beamline at BL-01C1of National Synchrotron Radiation Research Center (NSRRC, Hsinchu, Taiwan), respectively. The 1.5 GeV electron storage ring was operated on Top-Up mode with an injection period in 60 second The beam current (I_0) is 360 mA with a small current variation ($\Delta I_0/I_0$) of 0.05 %. Three gas-filled ion chambers were used in series to measure the intensities of the incident beam (I_0), the beam transmitted across the sample (I_t), and the beam subsequently transmitted across the reference foil (I_r). The third ion chamber was used in conjunction with the reference spectra of standard samples ($\mu_t^{ref} = \ln(I_t/I_r)$) of Co foil and Ru powder for energy calibration at Co *K*-edge and Ru *K*-edge, respectively. All the Co *K* and Ru *K*-edges XAS spectra of prepared samples were collected in a fluorescence mode (i.e. $\mu_F(E) = (I_F/I_0)$) by suing a Lytle detector equipped with Solar-Slits.

Data Subtraction of Co *K* and Ru *K*-edge XAS. The XAS data including the XANES and the EXAFS oscillations ($\chi(k)$), where *k* is the photoelectron wave number, were extracted and normalized according to the standard procedures of Athena program (with the code of AUTOBK algorithm 2.93) in the IFEFFIT package (version 1.2.10)[1-7]. Using a Hanning window function forward Fourier transformation (FFT) was performed on the EXAFS region of normalized XAS spectra with the selected *k* ranges for the Co *K* (from 3.5 to 13.9 $Å^{-1}$) and Ru *K*-edges (from 3.1 to 14.1 $Å^{-1}$) to generate the radial structure functions (RSF) in the radial space ranging from 1.0 to 6.0 Å.

XAS data analysis (model fitting). To conduct a XAS simulation, the reference structural information of standard Co_3O_4 (ICSD #9362), CoO (ICSD #9865), Ru metal (ICSD #41515), and RuC (ICSD #43671) crystals (obtained from the Inorganic Crystal Structure Database (ICSD) and WebAtoms Database) was implemented in FEFF6.20 program[8] in the IFEFFIT package (version 1.2.10)[1, 5, 6] to generate the theoretical bond paths of Co-Co, Co-O, Ru-C, and Ru-Ru. The model of simulating Co *K*-edge XAS data was based on the cadre of Co_3O_4 and CoO crystals. In the Co_3O_4 model the first two nearest shells are Co-O and Co-Co bonds, that have 12 and 4 coordination neighbors in the interatomic distance R_{Co-O} and R_{Co-Co} of 1.956 Å and 3.334 Å, respectively. Furthermore, the short range cobalt to oxygen bond paths were generated using the structural information of CoO crystal by FEFF6.01 code[9]. Model of Ru and RuC structures were referred to the standard information depicted by Kempter, C. P. et al (1960)[10].

The obtained RSF function was analyzed using EXAFS simulation (Artemis kits) with appropriate models (the scattering paths of Co-Co, Co-O, Ru-Ru, and Ru-C bonding pairs) to determine the local structural parameters of Co and Ru NPs in the IFEFFIT program with the EFEE6.01 code[3, 11, 12]. The fitting parameters includes the interatomic bond distance (R_{ij}), phase shifts (Φ_{ij}), coordination numbers (N_j), amplitude reduction factor (S_i^2), effective wave backscattering amplitude ($F_j(k)$), and Debye-Waller factor (σ_j^2)) around X-ray excited atoms. To simplify the EXAFS fitting, the values of S_i^2 of Co and Ru atoms were fixed at 0.87 which was in good agreement with the theoretical estimation and can be used for different samples with central atoms in a similar chemical state (valence, coordination). Only single scattering paths were considered in fitting the experimental XAS data to prevent unexpected analytical errors (which may be due to the background noises or the multiple scattering effects

from the higher order shells). The model simulation of XAS fitting with metal substitution was conducted by incorporating appropriate constrains in a single coordination shell. To evaluate the local structural information around X-ray excited atoms, we adopted independent iterations to avoid the unexpected errors of direct correlation between structural parameters. The $k^3\chi(k)$ were fitted with all the possible scattering paths for the corresponding FT peaks, where structural parameters of σ_j^2, N_j, and the R_{ij} were treated as adjustable parameters.

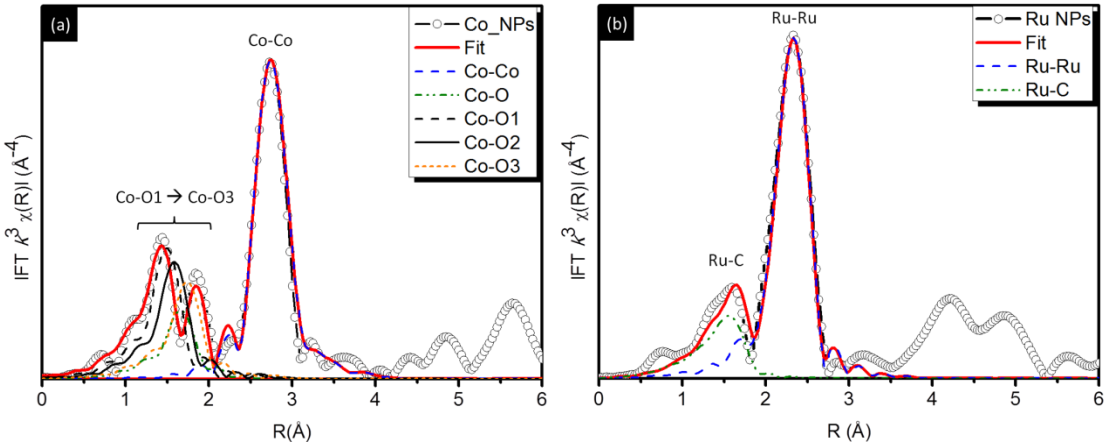

Fig. S1. The FT transformed extended X-ray absorption EXAFS spectra (lFT-k^3 χ(R)l) compared with the fitting curves of Co NPs (S1a) and Ru NPs(S1b).

The XAS fitting curves are compared with the FT transformed EXAFS spectra (lFT-k^3 χ(R)l) of Co and Ru NPs in Figure S1a and S1b, respectively. As can be seen, the fitting curves are in good agreement with that of experiment spectra, which suggesting that the proposed model are adequate for extracting the atomic structural parameters. The structural parameters are summarized in Table S1. Accordingly, the local structure of Co NPs consisted of Co_3O_4 and CoO phases. The coordination numbers of Co-Co and Co-O bond pairs are determined to be 0.8 and 2.4, respectively, which are 80% smaller than that of theoretical Co_3O_4 model. This deviation could be

attributed to the local disorder and the substantial surface defects of these ultra small Co NPs (~1.5 nm in diameter). In this environment, the local disorder is depicted by a negative Co-Co bond length displacement by 0.2 Å. The three additional Co-O coordination shells in the short radial range of |FT-k^3 χ(R)| is a direct evidence for the formation of oxygen bonding that presented at the highly hydrated Co NPs surface. From a density functional theory (DFT) calculation, we can notice that the highly hydrated Co_3O_4 have a substantial lower surface energy than that of anhydrous one[13]. Hereby, it is suggested that the surface of Co NPs was covered with a hydration layer due to the relatively high activity of Co NPs. This energy difference could be the driving force that leads to the disorder and displacement of Co-Co bond length. From XAS model analysis, the local structure of Ru NPs is described by Ru-Ru and Ru-C bond pairs. The former has a bond length of 2.67 Å with a CN_{Ru-Ru} of 6.3 and the later has a bond length of 2.05 Å with a CN_{Ru-C} of 3.5, respectively. The presence of Ru-C shell is an indication for the strong surface polymer bond resulting from the high surface free energy of Ru metal. The small CN_{Ru-Ru} refers to the loss of neighbouring atoms in a small nanoparticle.

Table S1. X-ray absorption spectroscopy measured the structure parameters of Co and Ru NPs. The residual factor (R-factor) for the two fitting batches is reduced to be smaller than 0.02 for the best fit.

	Co_3O_4		Co_3C_1				
Shell	R (Å)	CN	shell	R (Å)	CN	σ^2 (Å^2)	E_0
Co-O	2.03	0.8	Co-O	1.86	1.2		
Co-Co	3.08	2.4	Co-O	1.95	1.2	0.002	-0.5
			Co-O	2.11	1.2		

	Ru metal		Ru Carbide (RuC)				
shell	R	CN	shell	R	CN	σ^2 (Å^2)	E_0
Ru-Ru	2.67	6.3	Ru-C	2.05	3.5	0.007	-8.1

3. TEM analysis of Pt_S/Co_C and Pt_S/Ru_C nanocrystallites.

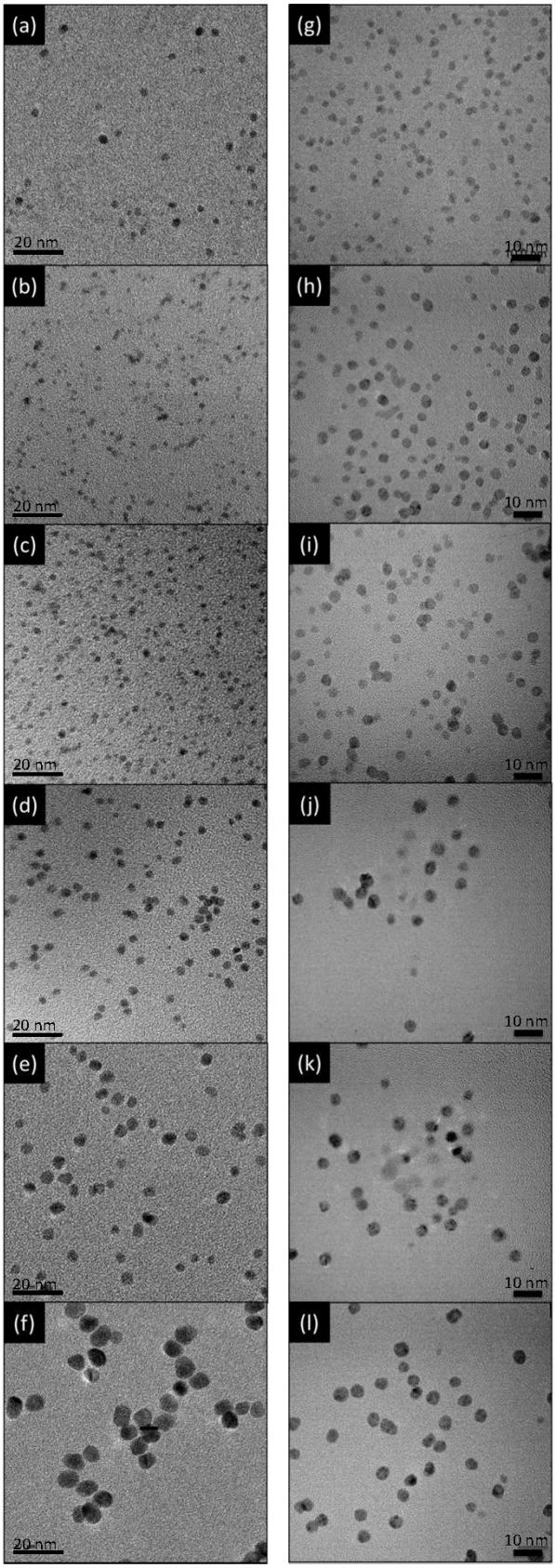

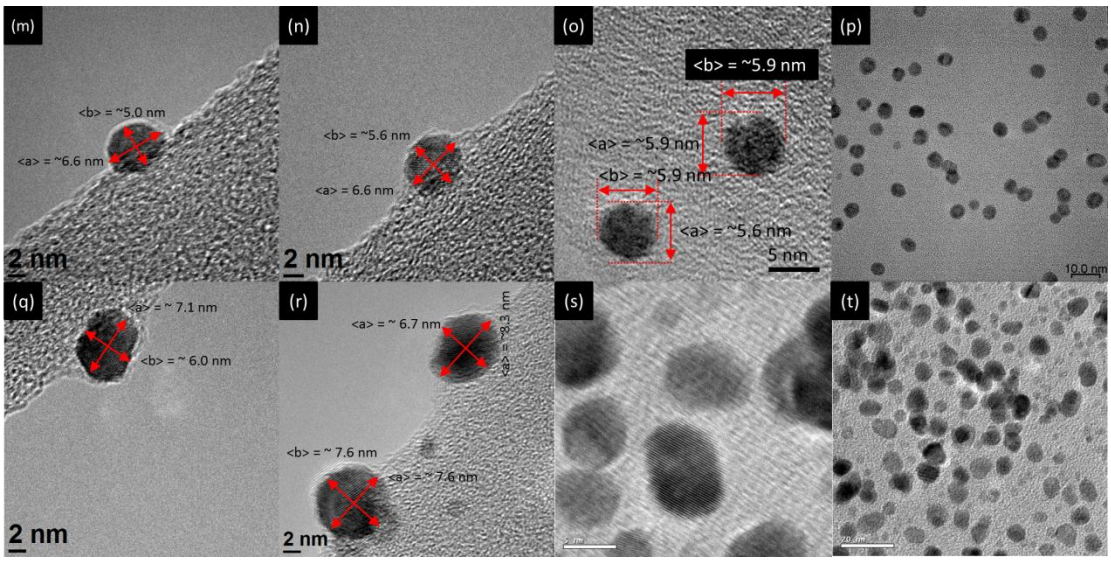

Fig. S2. Typical TEM images of Co cored (S2a-S2f) and Ru cored (S2g-S2l) NPs.(S2m – S2p) and (S2q – S2t) the TEM images of Pt_S/Ru_C and Pt_S/Co_C with 75 at% of Pt, respectively. The Scale bars in Fig. S2a – S2f and S2g – S2l are 20 and 10 nm, respectively.

2. XRD data collection for core-shell NCs

The XRD patterns of the Co_{core}-Pt_{shell} NPs were collected using a Mar345 imaging plate area detector and a Huber 8-circle diffractometer at BL-01C and BL-07A of the National Synchrotron Radiation Research Center (NSRRC). The XRD patterns of Ru_{core}-Pt_{shell} NPs were collected using a Quantum 210 CCD area detector and a sample alignment system at the NSRRC contract beamtime of BL-12B2 in SPring-8, Japan. The incident X-ray wavelength was tuned to 0.77743 Å (15.95 keV) using a Si(111) double crystal monochromator. The diffraction patterns of standard silicon and silver powders were collected to correct for the curvature of the detector and to calibrate the sample to detector distance, respectively.

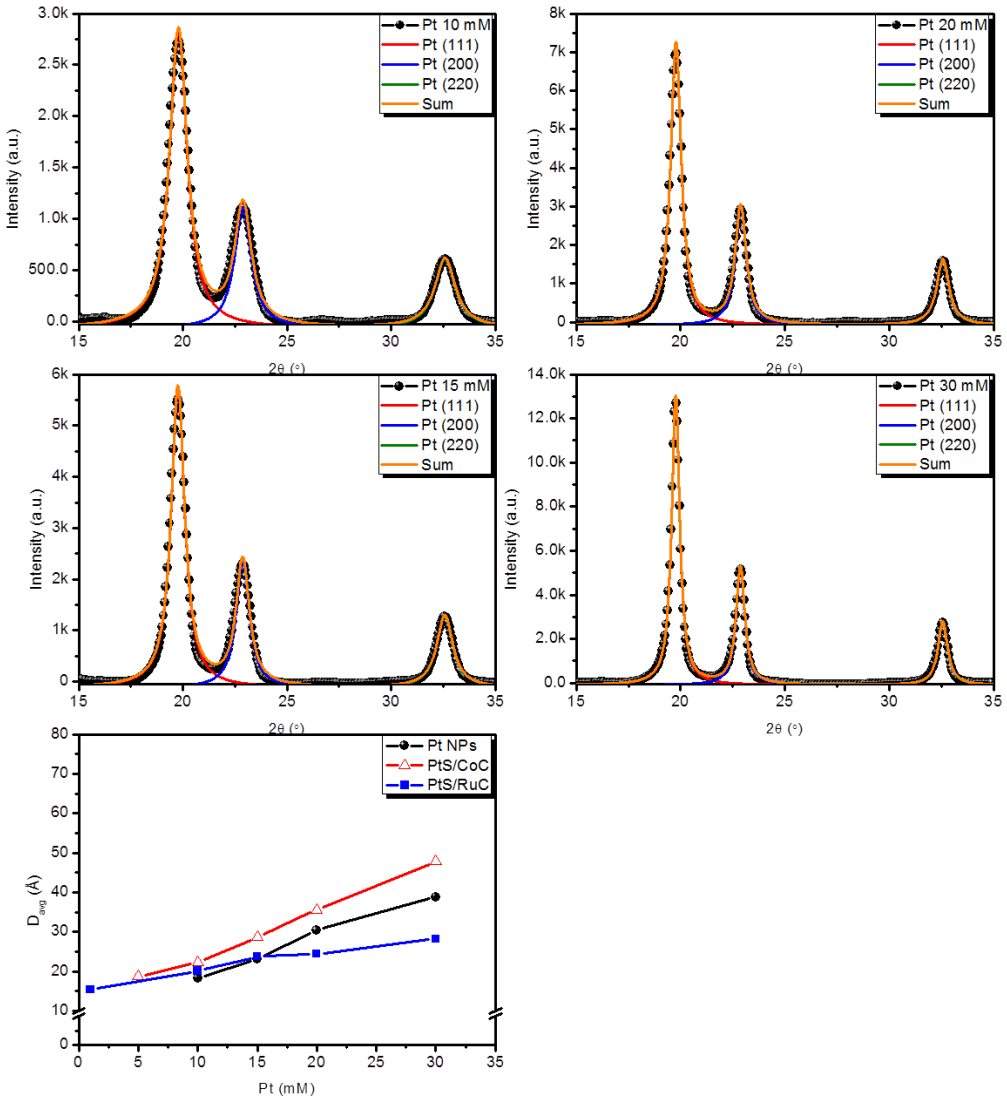

Figure S3. XRD patterns of monometallic Pt NPs synthesized by different Pt concentrations and the changes of average coherent length (D_{avg}) for Pt, Pt_S/Co_C, and Pt_S/Ru_C NPs with increasing Pt content.

3.1 Data collection and model analysis for Small angle X-ray Scattering spectra of core-shell NCs.

All SAXS data were collected at the In-Achromate superconducting wigglers (IASW) beamline at BL-23A of the National Synchrotron Radiation Research Center (NSRRC, Taiwan) with an incident X-ray beam wavelength of 0.8857 Å (14.0 keV). The SAXS data were corrected for sample transmission, background, and detector sensitivity, and normalized to the absolute scattering scale (scattering cross-section per unit sample volume $I(q)$). Samples (containing ~0.1 mg of NPs and ~1.0 wt% of PVP-40 in distilled water) were sealed in 3.0 mm thick stainless steel cells using two kapton films (~25 μm thick) for the X-ray windows. With the sample to detector distance of 2730 mm, the SAXS data were collected with an area detector over a Q-range from 0.01 to 0.397 $Å^{-1}$. The resulting scattering functions were analyzed using a two-component SAXS model consisting of fractal aggregate[15, 16] and core-shell NPs models[17].

The least-square fitting curve (solid line), the fitting curve of the fractal model (dashed line), and the core-shell cylinder model with Shultz distribution of shell thickness (dash-dotted line) are shown in Figure S3. As depicted, all experimental data fits well with the proposed model. Based on the fitting parameters (Table S3), the inter-particle fractal dimension (D_F) for Pt_S/Ru_C increases from 3.58 to 3.85 while the inter-particle scattering correlation length (ξ) remains unchanged (between ~25 to ~35 Å) at Pt contents from 9.1 to 75 at%. Given that the ξ of Pt_S/Ru_C is similar to the average particle size, it is suggested that the plane surface scattering interference (D_F > 3.0) could originated from the individual particle scattering contributions from the anisotropically grown flat surfaces. On the other hand, the inter-particle aggregation

of the Pt_S/Co_C NCs progressively increased with Pt content. This increase in D_F indicates that the aggregation of nanoparticles. It is possible that the loss of heterogeneous surface regions (A_{NPs}) in conjunction with the polymer ligands is due to the aggregation of these NCs. With increasing particle size, the A_{NPs} would decrease inversely with particle size (r). Therefore, it (the reduced specific surface area of NCs by increased bulk dimension) would increase the excess surrounding the polymer molecules, and result in NCs aggregation. An inter-particle D_F of ~2.0 with a ξ of 60 to 75 Å shows that the Pt_S/Co_C NCs would be mostly packed into 2-D random clusters that contain 9 to 16 individual scattering blocks (nanoparticles).

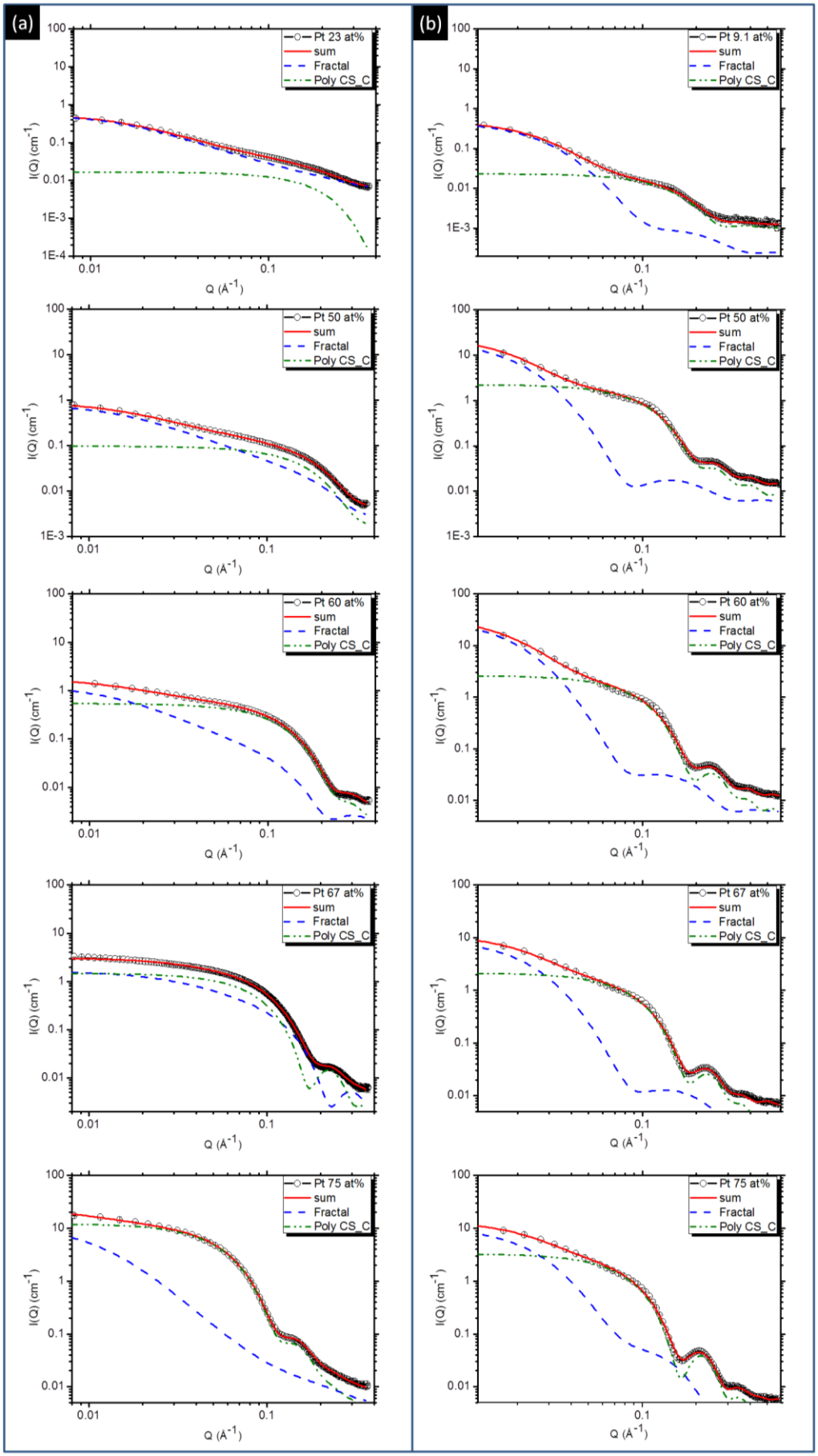

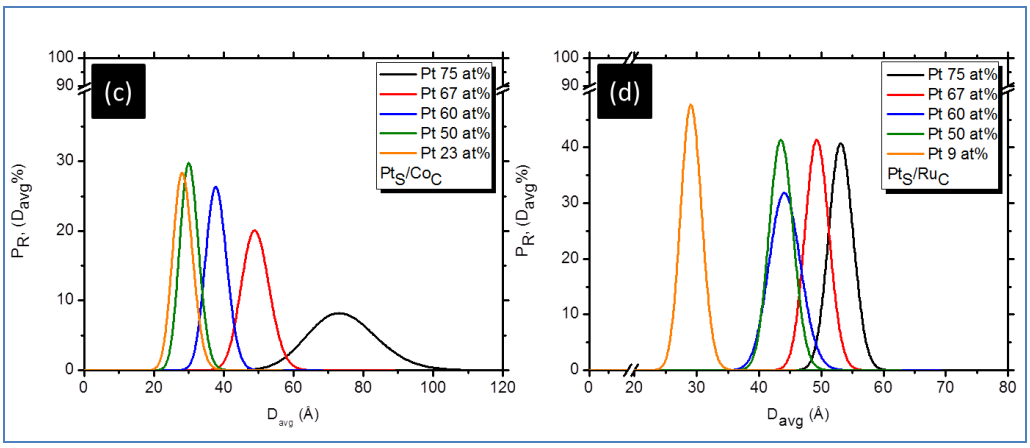

Fig. S4. Small angle X-ray scattering fitting curves from freshly prepared Pt_S/Co_C (a) and Pt_S/Ru_C (b) core-shell NCs. The Pt atoms of the NCs are labelled in the inset of each sub-figure. Polydispersity (P_R) of (c) Pt_S/Co_C and (d) Pt_S/Ru_C NPs.

Table S3. The inter-particle structural parameters of the electrocatalysts determined from fitting the experimental SAXS spectra with the proposed binary models are shown below.

Pt_s/Co_c				Pt_s/Ru_c			
Pt (at%)	D_F	R_B (Å)	ξ (Å)	Pt (at%)	D_F	R_B (Å)	ξ (Å)
23.1	1.78	9.55	61.65	9.1	3.58	10.57	25.58
50	1.75	11.87	65.49	50	3.68	10.63	31.78
60	1.95	18.52	67.31	60	3.79	12.38	30.52
66.7	1.95	19.39	62.72	66.7	3.78	12.91	28.59
75	2.51	8.15	75.61	75	3.85	16.97	25.87

Table S4. The SAXS determined intra-particle structure parameters of the core-shell NCs.

3.2 Estimation on surface to bulk ratio of nanoparticles

From a geometric standpoint, the surface to bulk ratio (ρ_{S-V}) for a particle can be estimated by using the following equation:

$$\rho_{S-V} = \frac{n_S}{n_t} \ldots (S2)$$

where n_S and n_t denote the number of surface atoms and total number of atoms, respectively. The n_S can be determined by dividing the occupied area ($P_S \times S'$, P_S denotes the surface atomic packing factor of a surface, and the surface area of the particle S' is equal to $4\alpha\pi R^2$ with radius R) by the cross section area of particle (πr^2, where r denotes the radius of the atom). For a particle, S' can be determined by multiplying the surface area of the spherical particle by a shape modification factor (α) that considers the extent of interfacet truncation. Therefore we can determine n_s by using Eq. S3.

$$n_S = P_S \frac{S'}{\pi r^2} = P_S \frac{4\alpha\pi R^2}{\pi r^2} = 4\alpha P_S \frac{R^2}{r^2} \ldots (S3)$$

The volume of a particle occupied by atoms (V_L) can be calculated by combining the half volume of the surface atoms ($0.5 \times n_S \times V_a$) and the volume of the interior atoms ($n_i \times V_a$), where V_a denotes the atom volume. If a particle has a volume of V_P, the occupied volume can be presented as follows by adopting a bulk lattice atomic packing factor, P_L (Eq. S4).

$$V_L = P_L \times V_P \ldots (S4)$$

By combining Eq. (S3) and Eq. (S4), we can obtain the following relationship:

$$V_L = n_i V_a + \frac{1}{2} n_S V_a = P_L V_P \Rightarrow n_i + \frac{1}{2} n_S = P_L \frac{V_P}{V_a} = P_L \frac{R^3}{r^3} \ldots (S5)$$

Here, the total number of atoms in a particle can be represented as $n_t = n_i + n_S$. According to Eq. (S3) and Eq. (S5), n_t can be represented as:

$$n_t = P_L \frac{R^3}{r^3} + 2\alpha P_S \frac{R^2}{r^2} \ldots (S6)$$

therefore, ρ_{S-V} is obtained from the following numerical representation:

$$\frac{n_S}{n_t} = \frac{4\alpha P_S \frac{R^2}{r^2}}{P_L \frac{R^3}{r^3} + 2\alpha P_S \frac{R^2}{r^2}} = \frac{4\alpha P_S}{P_L \frac{R}{r} + 2\alpha P_S} \quad ...(S7)$$

Because the shape factor parameters and the packing factors are dominated by particle shape, ρ_{S-V} is inversely proportional to the radius of the particle (R). This relationship is represented in Figure S5.

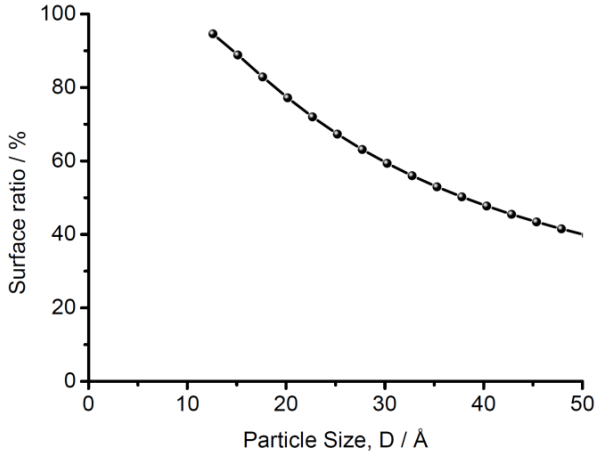

Figure S5. The surface to bulk ratio of sphere nanoparticles as a function of particle size. For spherical particles $\alpha = 1$, and for ellipsoid particles $1 < \alpha < 2$.

3.3. Estimation of the theoretical surface area (TSA) of core-shell NCs

To simplify the estimation, the NCs are draw as a disk-like particle corresponding to a surface area (A_{NPs}) of $2\pi R_{NPs} \times L_{NPs} + 2 \times \pi R_{NPs}^2$. The parameters of R_{NPs}^2 and L_{NPs} denote the radius and length of particle. Consider the core-shell structure with the thicknesses of face shell (T_F) and radial shell (T_R), the R_{NPs} and L_{NPs} should be presented as $R_C + 2 \times T_R$ and $L_C + 2 \times T_F$, respectively. Accordingly, the surface area of each NCs is derived as $A_{NPs} = 2\pi(R_C + 2T_R) \times (L_C + 2T_F) + 2 \times \pi (R_C + 2T_R)^2$ and

thus the weight of each particle is represented as $M_{NPs} = V_{NPs} \times \rho_{NPs}$. The parameters of ρ_{NPs} and V_{NPs} denote the mass density and volume of individual particle. Consequently, the theoretical specific surface area (TSA) per gram of NCs could be estimated by adopting the density of Pt, Ru, and Co_3O_4 into following equation:

$$TSA = \frac{1}{M_{NPs}} \times A_{NPs} = \frac{A_{NPs}}{V_{NPs} \times \rho_{NPs}} \quad ...(S8)$$

where the volume of disk-like particle is represented as $V_{NPs} = \pi (R_C + 2T_R)^2 \times (L_C + 2T_F)$ and the mass density can be estimated by considering the weighting of two components in the NCs.

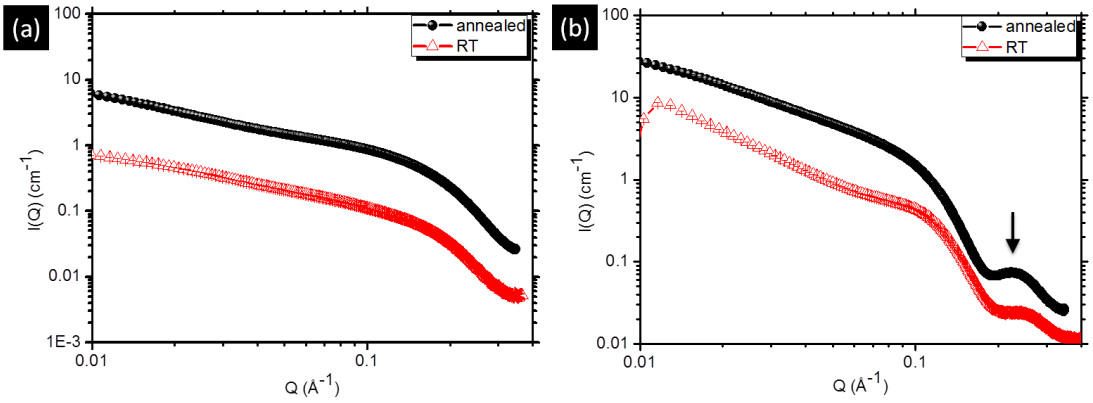

Figure S6. The SAXS spectra of the (a) Pt_S/Co_C and (b) Pt_S/Ru_C core-shell NPs with pre-treatment for ECSA measurements are shown here. The fitting curves of the two spectra are not presented.

Table S5. The inter-particle structure parameters (determined by SAXS) of the core-shell nanoparticles with ECSA pre-treatment (annealed) are shown.

NCs	Sample condition	D_F	R_B (nm)	ξ (nm)	$2R_C$ (nm)	L_C (nm)	T_R (nm)	T_F (nm)	P_R (%)	TSA (m^2 g^{-1})
Pt_S/Co_C	Fresh	1.95	1.93	6.73	3.15	1.58	0.41	0.30	10.7	190.7
	Annealed	2.21	1.97	10.16	2.82	1.63	0.40	0.30	8.0	188.7
Pt_S/Ru_C[*]	Fresh	3.81	0.92	1.93	2.70	2.04	0.92	0.42	10.2	94.3
	Annealed	3.76	0.88	3.03	2.75	2.12	0.91	0.42	12.6	99.3

R_B denotes the radius of the polymer blended individual scattering body. ξ represents the correlation length between the scattering bodies. R_C (with a polydispersity of P_R) and L_C denote the radius and length of the core. T_F and T_R denote the thickness of the face and radial shell, respectively.

[*] denotes Pt_S/Ru_C NCs with a Pt content of 55 at%.

According to the SAXS fitting results in Table S5, we can estimate the effect of thermal treatment on the TSA of the two core-shell NPs. The results of TSA are given in the last column of Table S5. It is clearly shown that the volume of the two types of NPs is almost identical after the annealing treatment. It is therefore suggested that the interparticle sintering could be ruled out from the differences of ECSA between the two NPs.

References

1. M. Newville, P. Livins, Y. Yacoby, J. J. Rehr and E. A. Stern, *Physical Review B* 1993, **47** 14126-14131.
2. M. Newville, Department of Physics, University ofWashington, Seattle, 1995.
3. M. Newville, *Journal of Synchrotron Radiation*, 2001, **8**, 322-324.
4. M. Newville, Cumulant Expansion Fitting, Accessed July 20th, 2010.
5. Y.-T. Liu, M. K. Wang, T.-Y. Chen, P. N. Chiang, P. M. Huang and J.-F. Lee, *Environmental Science & Technology* 2006, **40** 7784-7789.
6. B. J. Hwang, L. S. Sarma, J. M. Chen, C. H. Chen, S. C. Shih, G. R. Wang, D. G. Liu, J. F. Lee and M. T. Tang, *Journal of the American Chemical Society* 2005, **127** 11140-11145.
7. P. J. Durham, in *X-Ray Absorption: Principles, Applications, Techniques of EXAFS, SEXAFS and XANES (Chemical Analysis: A Series of Monographs on Analytical Chemistry and Its Applications)*, eds. D. C. Koningsberger and R. Prins, John Wiley & Sons, New York, 1998, pp. 53-81.
8. A. L. Ankudinov, B. Ravel, J. J. Rehr and S. D. Conradson, *Physical Review B*, 1998, **58** 7565-7576.
9. J. J. Rehr and R. C. Albers, *Physical Review B*, 1990, **41**, 8139-8149.
10. C. P. Kempter and M. R. Nadler, *Journal of Chemical Physics*, 1960, **33**, 1580-1581.
11. B. Ravel and M. Newville, *Journal of Synchrotron Radiation*, 2005, **12**, 537-541.
12. B. Ravel, *Journal of Synchrotron Radiation*, 2001, **8**, 314-316.
13. A. Navrotsky, C. Ma, K. Lilova and N. Birkner, *Science*, 2010, **330**, 199-201.
14. M. Radermacher, T. Wagenknecht, A. Verschoor and J. Frank, *Journal of Microscopy*, 1987, **146 (Pt 2)**, 113-136.
15. J.-M. Lin, T.-L. Lin, U.-S. Jeng, Y.-J. Zhong, C.-T. Yeh and T.-Y. Chen, *Journal of Applied Crystallography*, 2007, **40**, s540-s543.
16. J. Teixeira, *Journal of Applied Crystallography*, 1988, **21**, 781-785.
17. P. Bartlett and R. H. Ottewill, *Journal of Chemical Physics*, 1992, **96**, 3306.